IOPscience iopscience.iop.org

Home Search Collections Journals About Contact us My IOPscience

Magnetic and orbital correlations in a two-site molecule

This article has been downloaded from IOPscience. Please scroll down to see the full text article.

2006 J. Phys.: Condens. Matter 18 7449

(http://iopscience.iop.org/0953-8984/18/31/036)

View the table of contents for this issue, or go to the journal homepage for more

Download details:
IP Address: 129.252.86.83
The article was downloaded on 28/05/2010 at 12:35

Please note that terms and conditions apply.

INSTITUTE OF PHYSICS PUBLISHING JOURNAL OF PHYSICS: CONDENSED MATTER

J. Phys.: Condens. Matter **18** (2006) 7449–7469 doi:10.1088/0953-8984/18/31/036

Magnetic and orbital correlations in a two-site molecule

Marcin Raczkowski[1,2], **Raymond Frésard**[2] **and Andrzej M Oleś**[1]

[1] Marian Smoluchowski Institute of Physics, Jagellonian University, Reymonta 4, PL-30059 Kraków, Poland
[2] Laboratoire CRISMAT, UMR CNRS–ENSICAEN(ISMRA) 6508, 6 Boulevard du Maréchal Juin, F-14050 Caen, France

E-mail: M.Raczkowski@if.uj.edu.pl, Raymond.Fresard@ensicaen.fr and A.M.Oles@fkf.mpg.de

Received 24 March 2006, in final form 21 June 2006
Published 21 July 2006
Online at stacks.iop.org/JPhysCM/18/7449

Abstract
We analyse the role of orbital degeneracy in possible magnetic and orbital instabilities by solving exactly a two-site molecule with two orbitals of either e_g or t_{2g} symmetry at quarter-filling. As a generic feature of both models one finds that the spin and orbital correlations have opposite signs in the low-temperature regime when the orbitals are degenerate, in agreement with the Goodenough–Kanamori rules. While Hund's exchange coupling J_H induces ferromagnetic spin correlations in both models, it is more efficient for t_{2g} orbitals where the orbital quantum number is conserved along the hopping processes. We show that the ground state and finite temperature properties may change even qualitatively with increasing Coulomb interaction when the crystal field splitting of the two orbitals is finite, and the Goodenough–Kanamori rules may not be followed.

(Some figures in this article are in colour only in the electronic version)

1. Introduction

The Hubbard model has been employed for a long time as the conceptually simplest model which might explain metallic ferromagnetism of itinerant electrons [1, 2] and localization due to Coulomb repulsion [3]. Unlike initially expected, this model does not easily yield ferromagnetism on the hypercubic lattice and some additional conditions have to be satisfied to stabilize a ferromagnetic (FM) phase. As one of very few exact result in this many-body problem, Nagaoka established long ago [4] that in the limit of infinite local Coulomb interaction $U = \infty$, a single hole doped into a half-filled system leads to the FM ground state. There are several indications that this remains valid for a finite concentration of holes [5, 6]. Nevertheless the ground state of the Hubbard model on the square lattice may only be FM for values of U far larger than the bandwidth [7]. Ferromagnetism may be also promoted by a particular lattice

or band structure [6], or even by disorder [8]. Lieb was the first to show that a half-filled flat band induces a finite magnetization [9]. Furthermore, Hirsch and others have focused on the effect of additional off-diagonal matrix elements of the Coulomb interaction [10].

A major step towards understanding the physics of metallic ferromagnetism in transition metals such as Fe, Co, and Ni, was the suggestion that orbital degeneracy might play a crucial role. It was first pointed out by Slater *et al* [11] and then stressed by van Vleck [12] that in the presence of degenerate orbitals, Hund's exchange coupling J_{H} favours local triplet spin configurations of two electrons occupying different orbitals. This has important consequences for ferromagnetism as local moments are formed and thus J_{H} helps to stabilize magnetic phases, including the FM one [13]. Roth examined the doubly degenerate model at quarter-filling in three dimensions [14]. She found that the ground state is a spin triplet and orbital singlet for two sites, i.e., the system forms an orbital superlattice structure in which two sublattices have different orbitals occupied by electrons at each of them. This interrelation between staggered orbital order and spin ferromagnetism was next emphasized by Kugel and Khomskii [15], who derived an effective strong coupling Hamiltonian with coupled spin and orbital degrees of freedom, extended further by Cyrot and Lyon-Caen [16] who included on-site pair hopping, and by Inagaki [17]. These seminal papers started a new field: spin–orbital physics in correlated transition metal oxides [18], where superexchange models derived in the strong coupling regime provide a theoretical background for understanding both magnetic and optical properties [19]. Numerous spin–orbital models have been derived in the regime of large Coulomb interactions, for systems with both $\mathrm{e_g}$ [20] and with $\mathrm{t_{2g}}$ [21] orbital degrees of freedom, and these are currently being investigated.

While systems of higher dimensionality are clearly the ones of most interest [22, 23], significant insight into the complementary behaviour of spin and orbital degrees of freedom was obtained in a one-dimensional (1D) model. Indeed, many of the essential features of such 1D systems were established by quantum Monte Carlo simulations [24], exact diagonalization (ED) studies [25–27], the combination of these two approaches [28], and the Density Matrix Renormalization Group (DMRG) method [29]. Spin, charge, and orbital correlations in the 1D Hubbard model with $\mathrm{t_{2g}}$ orbitals at several densities have been also examined in a very recent study by Xavier *et al* [30], which combines the DMRG and the Lanczos techniques.

Unfortunately, in a vast majority of studies, a conceptually simplified model, i.e., the degenerate Hubbard model with equivalent orbitals [22] or at best with different bandwidth obtained with diagonal hopping [23], has been investigated so far. However, it has been recently shown within dynamical mean field theory that a finite on-site hybridization between orbitals enhances the charge and orbital fluctuations and plays a significant role especially for the orbital-selective Mott transition [31]. In fact, a proper description of a system with $\mathrm{e_g}$ orbitals involves a more complex kinetic energy Hamiltonian as in this case the orbital flavour during the intersite hopping is not conserved, and this is likely to lead to partial orbital polarization which is expected to strongly modify the magnetic instabilities [32, 33], resulting in a rich phase diagram. In addition only little is known in analytic form about these models, besides expansions in hopping parameter t around the atomic limit which result in the celebrated Goodenough–Kanamori rules [34, 35] and spin–orbital models. In particular cases, such as half-filling in two-band models, they corroborate the results obtained from weak coupling approaches, and therefore gaining further qualitative insight into the corresponding problems is unlikely. In contrast, at quarter-filling, weak coupling approaches are at odds with the strong coupling expansions [32], and the situation remains controversial. Fortunately this case can be studied rigorously on the analytical level, both for $\mathrm{e_g}$ and $\mathrm{t_{2g}}$ orbitals, in a two-site molecule.

The paper is organized as follows. First, we introduce a *realistic* model with two $\mathrm{e_g}$ orbitals and compare it with the one for $\mathrm{t_{2g}}$ orbitals in section 2. Second, the solutions for

both models are given and compared with each other in section 3. Thereby, we identify characteristic differences in the behaviour of both orbital degrees of freedom [36]. Furthermore, in section 3 we verify whether the phenomenon of a complementary behaviour of the spin and orbital flavours is also a characteristic feature of this particular case by analysing spin and pseudospin correlation functions. Comparisons to strong coupling expansions are presented as well. Next, in section 4 we investigate the influence of finite crystal field splitting on the ground state properties. Finally, section 5 summarizes the paper and gives general conclusions.

2. Model Hamiltonian for e_g and for t_{2g} orbitals

The magnetic and orbital instabilities within the e_g band become especially relevant in the context of doped nickelates $La_{2-x}Sr_xNiO_4$ (LSNO), where interesting novel phases including the stripe order were discovered [37]. Even though doped nickelate LSNO is isostructural with its cuprate counterpart $La_{2-x}Sr_xCuO_4$, its electronic degrees of freedom are more complicated. In fact, a realistic Hamiltonian for LSNO must contain, besides the $x^2 - y^2$ orbital states which mainly determine the properties of the cuprates, also the $3z^2 - r^2$ orbital states, so as to account for the actual filling with two holes and for the high-spin state ($S = 1$) in the stoichiometric compound. Such a model of interacting e_g electrons in the (a, b) plane may be written as follows,

$$\mathcal{H} = H_{\rm kin} + H_{\rm int} + H_{\rm cf}, \tag{1}$$

with two orbital flavours, $|x\rangle \sim x^2 - y^2$ and $|z\rangle \sim 3z^2 - r^2$, forming a basis in the orbital space. The kinetic energy is described by

$$H_{\rm kin} = \sum_{\langle ij\rangle}\sum_{\alpha\beta\sigma} t_{ij}^{\alpha\beta} c_{i\alpha\sigma}^{\dagger} c_{j\beta\sigma}, \qquad t_{ij}^{\alpha\beta} = -\frac{t}{4}\begin{pmatrix} 3 & \pm\sqrt{3} \\ \pm\sqrt{3} & 1 \end{pmatrix}, \tag{2}$$

where t stands for an effective $(dd\sigma)$ hopping matrix element due to the hybridization with oxygen orbitals on Ni–O–Ni bonds, and the off-diagonal hopping t_{ij}^{xz} along a and b axes depends on the phase of the $|x\rangle$ orbital along the considered cubic direction.

For our purpose it is most convenient to consider an e_g orbital basis consisting of a directional orbital $|\zeta\rangle$ along the molecular bond and a planar orbital $|\xi\rangle$ orthogonal to $|\zeta\rangle$ [28]. Pairs of such orthogonal orbitals defining a new basis might be obtained by the following transformation of the original orbital basis $\{|x\rangle, |z\rangle\}$,

$$\begin{pmatrix} |\zeta\rangle \\ |\xi\rangle \end{pmatrix} = \begin{pmatrix} \cos\frac{\theta}{2} & \sin\frac{\theta}{2} \\ -\sin\frac{\theta}{2} & \cos\frac{\theta}{2} \end{pmatrix}\begin{pmatrix} |z\rangle \\ |x\rangle \end{pmatrix}, \tag{3}$$

with the angle $\theta = \pm 2\pi/3$ depending on whether one considers the bond along the a or b axis. This rotation leads to a simple diagonal form of the hopping matrix,

$$t_{ij}^{\zeta\xi} = -t\begin{pmatrix} 1 & 0 \\ 0 & 0 \end{pmatrix}, \tag{4}$$

allowing only for intersite transitions between two directional $|\zeta\rangle$ orbitals along each bond [38]. We compare this case with a frequently studied degenerate Hubbard model with equivalent orbitals. Such a model describes the dynamics of two active t_{2g} orbitals, for example, for a molecular bond along the a axis, $|\zeta\rangle \sim |xz\rangle$ and $|\xi\rangle \sim |xy\rangle$, so that the hopping matrix is diagonal,

$$t_{ij}^{\zeta\xi} = -t\begin{pmatrix} 1 & 0 \\ 0 & 1 \end{pmatrix}. \tag{5}$$

Pairs of orthogonal orbitals $\{|\zeta\rangle, |\xi\rangle\}$ used in both models are presented in figure 1.

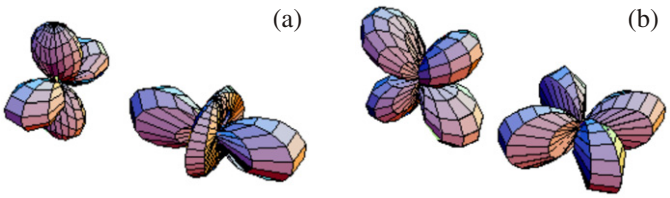

Figure 1. Pairs of orthogonal orbitals $\{|\zeta\rangle, |\xi\rangle\}$ for a molecular bond along the a axis for (a) e_g orbitals, and (b) t_{2g} orbitals.

The electron–electron interactions are described by the on-site terms, which we write in the following form [39],

$$H_{\rm int} = U\sum_i (n_{ix\uparrow}n_{ix\downarrow} + n_{iz\uparrow}n_{iz\downarrow}) + \left(U - \tfrac{5}{2}J_{\rm H}\right)\sum_i n_{ix}n_{iz} - 2J_{\rm H}\sum_i \mathbf{S}_{ix}\cdot\mathbf{S}_{iz} + J_{\rm H}\sum_i (c^\dagger_{ix\uparrow}c^\dagger_{ix\downarrow}c_{iz\downarrow}c_{iz\uparrow} + c^\dagger_{iz\uparrow}c^\dagger_{iz\downarrow}c_{ix\downarrow}c_{ix\uparrow}). \tag{6}$$

Here U and $J_{\rm H}$ stand for the intraorbital Coulomb and Hund's exchange elements, whereas $n_{i\alpha} = \sum_\sigma n_{i\alpha\sigma}$ is the electron density at site i in the $\alpha = x, z$ orbital state.

The last term $H_{\rm cf}$ stands for the uniform crystal-field splitting between $|x\rangle$ and $|z\rangle$ orbitals along the c axis,

$$H_{\rm cf} = \tfrac{1}{2}E_0\sum_{i\sigma}(n_{ix\sigma} - n_{iz\sigma}). \tag{7}$$

The splitting of two e_g orbitals occurs due to the tetragonal Jahn–Teller distortion of the NiO_6 octahedron. In La_2NiO_4, however, the octahedron, with the Ni–O–Ni bond lengths being 1.95 (2.26) Å in-plane (out-of-plane) [40], respectively, is much less distorted than the CuO_6 octahedron with 1.89 and 2.43 Å bond lengths in La_2CuO_4 [41], which reflects the difference in electron filling. In what follows we consider only a realistic positive E_0 favouring, due to elongated octahedra, the $|z\rangle$ occupancy over the $|x\rangle$ occupancy by the e_g electrons in doped compounds.

3. Physical properties at orbital degeneracy

3.1. Classification of eigenstates using the symmetry properties

In this section we present an exact solution of a two-site molecule at quarter-filling with two degenerate orbitals of either e_g or t_{2g} symmetry. Although it is straightforward to solve the present problem numerically, it is more instructive to find the solution analytically. During this process several important aspects will be clarified.

While the total spin operator commutes with the Hamiltonian and its z-component can be used to label the eigenstates, this does not hold for the total orbital pseudospin operator $\mathbf{T} = \sum_i \mathbf{T}_i$, where its three components are given by

$$\mathbf{T}_i = \left\{\mathcal{T}_i^+, \mathcal{T}_i^-, \mathcal{T}_i^\zeta\right\} = \left\{\sum_\sigma c^\dagger_{i\xi\sigma}c_{i\zeta\sigma}, \sum_\sigma c^\dagger_{i\zeta\sigma}c_{i\xi\sigma}, \tfrac{1}{2}\sum_\sigma (n_{i\xi\sigma} - n_{i\zeta\sigma})\right\}. \tag{8}$$

In order to distinguish the third component of the pseudospin from that conventionally used for a bond along the c axis ($\mathcal{T}_i^z$), we have labelled it with the ζ index. Note however that in contrast to the spin operator S^z, the ζ-component of the pseudospin operator,

$$\mathcal{T}^\zeta = \sum_i \mathcal{T}_i^\zeta, \tag{9}$$

does not commute with the Hamiltonian (1), so the states with different values of this observable mix with each other. Nevertheless, we will use its eigenvalues together with the z-component S^z of the total spin operator $\mathbf{S}$ to specify multiparticle states in terms of which we write the Hamiltonian. It is straightforward to construct all 28 states explicitly; they are listed in appendix A.

In the high-spin subspaces $S^z = \pm 1$, the Hamiltonian (1) is decomposed into a zero 2×2 matrix $H_{0\sigma}$ involving the two $|\Psi_{\alpha\sigma}\rangle$ states with $T^\zeta = \pm 1$, and two 2×2 matrices:

$$H_{1\sigma} = \left(\langle\Psi^+_{1\sigma}|, \langle\Psi^-_{2\sigma}|\right) \begin{pmatrix} 0 & t_{\zeta\zeta} - t_{\xi\xi} \\ t_{\zeta\zeta} - t_{\xi\xi} & U - 3J_{\mathrm{H}} \end{pmatrix} \begin{pmatrix} |\Psi^+_{1\sigma}\rangle \\ |\Psi^-_{2\sigma}\rangle \end{pmatrix}, \tag{10}$$

and

$$H_{2\sigma} = \left(\langle\Psi^-_{1\sigma}|, \langle\Psi^+_{2\sigma}|\right) \begin{pmatrix} 0 & t_{\zeta\zeta} + t_{\xi\xi} \\ t_{\zeta\zeta} + t_{\xi\xi} & U - 3J_{\mathrm{H}} \end{pmatrix} \begin{pmatrix} |\Psi^-_{1\sigma}\rangle \\ |\Psi^+_{2\sigma}\rangle \end{pmatrix}. \tag{11}$$

Now we are left with the $S^z = 0$ subspace. In the $S = 1$ sector one recovers the same eigenenergies: two zeros corresponding to the above $T^\zeta = \pm 1$ localized states with $T^\zeta = \pm 1$, and the eigenvalues following from the matrices $H_{1\sigma}$, and $H_{2\sigma}$. In the $S = 0$ subspace, using the states with $T^\zeta = \pm 1$, the following Hamiltonian matrices are found in addition:

$$H_3 = \left(\langle\Phi^-_1|, \langle\Phi^+_2|, \langle\Phi^+_3|, \langle\Phi^-_4|\right) \begin{pmatrix} 0 & 2t_{\zeta\zeta} & 0 & 0 \\ 2t_{\zeta\zeta} & U & J_{\mathrm{H}} & 0 \\ 0 & J_{\mathrm{H}} & U & 2t_{\xi\xi} \\ 0 & 0 & 2t_{\xi\xi} & 0 \end{pmatrix} \begin{pmatrix} |\Phi^-_1\rangle \\ |\Phi^+_2\rangle \\ |\Phi^+_3\rangle \\ |\Phi^-_4\rangle \end{pmatrix}, \tag{12}$$

and

$$H_4 = \left(\langle\Phi^-_2|, \langle\Phi^-_3|\right) \begin{pmatrix} U & J_{\mathrm{H}} \\ J_{\mathrm{H}} & U \end{pmatrix} \begin{pmatrix} |\Phi^-_2\rangle \\ |\Phi^-_3\rangle \end{pmatrix}. \tag{13}$$

Finally, in the sector with $T^\zeta = 0$, the Hamiltonian matrices read

$$H_5 = \left(\langle\Phi^+_7|, \langle\Phi^-_8|\right) \begin{pmatrix} U - J_{\mathrm{H}} & t_{\zeta\zeta} + t_{\xi\xi} \\ t_{\zeta\zeta} + t_{\xi\xi} & 0 \end{pmatrix} \begin{pmatrix} |\Phi^+_7\rangle \\ |\Phi^-_8\rangle \end{pmatrix}, \tag{14}$$

$$H_6 = \left(\langle\Phi^-_7|, \langle\Phi^+_8|\right) \begin{pmatrix} U - J_{\mathrm{H}} & t_{\zeta\zeta} - t_{\xi\xi} \\ t_{\zeta\zeta} - t_{\xi\xi} & 0 \end{pmatrix} \begin{pmatrix} |\Phi^-_7\rangle \\ |\Phi^+_8\rangle \end{pmatrix}. \tag{15}$$

3.2. Eigenenergies for t_{2g} orbitals

Let us consider first a model with two active and equivalent $\mathrm{t_{2g}}$ orbitals, as depicted in figure 1(b). The third orbital may be neglected in various contexts: (i) either in a d^1 configuration when a crystal field raises the energy of the third orbital above the other two we consider here, or (ii) in a d^3 low-spin configuration when a crystal field lowers the energy of the third orbital below the other two (the former one being filled), or (iii) in a d^5 low-spin configuration when a crystal field lowers the energy of the third orbital below the other two, in which case one meets the problem of one hole in two orbitals. Of the few layered perovskites that may correspond to these cases let us mention $\mathrm{NdSrCrO_4}$ [42]. We note that the distortions in layered perovskites differ from the ones in cubic perovskites, where they are typically trigonal. For this model every matrix in equations (12)–(15) can be easily diagonalized and the corresponding eigenvalues are listed in appendix B. For clarity we have used the symmetry and classified them into triplet ($S = 1$) and singlet ($S = 0$) subspaces.

To get more insight into the competition between the tendencies towards the antiferromagnetic (AF) and FM ground states, we now discuss the lowest energy eigenstates in the strong coupling (large-U) limit. As expected, the lowest energy,

$$E^{\mathrm{t_{2g}}}_{T_0} = \tfrac{1}{2}\left(U - 3J_{\mathrm{H}} - \sqrt{(U - 3J_{\mathrm{H}})^2 + 16t^2}\right), \tag{16}$$

Table 1. Lowest eigenenergies of the model (1) for t_{2g} orbitals at $U = 8t$, obtained for the representative values of $J_H = 0$, $U/8$ and $U/4$. The eigenstates $|n\rangle$ are specified by the total spin S_n and the expectation value of the ζ-component of the total pseudospin $\mathcal{T}^\zeta$ (9). Triplet states with $S_n = 1$ have three components $S_n^z = \pm 1, 0$.

$J_H = 0$			$J_H = U/8$			$J_H = U/4$		
E_n/t	S_n	T_n^ζ	E_n/t	S_n	T_n^ζ	E_n/t	S_n	T_n^ζ
−0.4721	1	0	−0.7016	1	0	−1.2361	1	0
	0	±1	−0.5311	0	0	−0.6056	0	0
	0	0		0	0		0	0

obtained by the diagonalization of the matrix in equation (11), belongs to the spin triplet coexisting with the pseudospin singlet. In the case of strong on-site interorbital repulsion ($U - 3J_H \gg t$), the lowest high-spin energy (16) reads

$$E_{T_0}^{t_{2g}} \simeq -\frac{4t^2}{U - 3J_H}. \tag{17}$$

Note however that finite J_H could significantly reduce the value of the interorbital repulsion $U - 3J_H$, so that it would no longer be much larger than t. As a consequence, significant corrections to the above result obtained to second order in $t/(U - 3J_H)$ are expected in this case. Analogously, the lowermost low-spin energy results from the matrix in equation (12), which is degenerate with the one obtained from the matrix in equation (14),

$$E_{S_0}^{t_{2g}} = -\tfrac{1}{2}\left(U - J_H - \sqrt{(U - J_H)^2 + 16t^2}\right) \simeq -\frac{4t^2}{U - J_H}, \tag{18}$$

in the strong coupling regime.

Comparison of equation (18) with the lowest high-spin energy given by equation (17) allows one to draw interesting conclusions about conditions required for ferromagnetism. It is apparent that $E_{S_0}^{t_{2g}}$ and $E_{T_0}^{t_{2g}}$ are degenerate for $J_H = 0$. However, even infinitesimally small Hund's exchange coupling lifts this degeneracy and might give rise to spin ferromagnetism combined with the alternating orbital (AO) pseudospin correlation.

As an illustrative example, we present in table 1 the lowest eigenenergies E_n obtained from the ED of the Hamiltonian (1) for the t_{2g} orbitals in the strong coupling regime $U = 8t$ for a few values of J_H. We have specified them in terms of the total spin $S_n = 0, 1$. Another quantity used for the classification of states is the ζ-component of the total pseudospin operator; see equation (9). However, even in this case it is not a good quantum number being modified by the 'pair-hopping' processes from one orbital to the other present in equation (6). Indeed, in matrix (12), a sector consisting of $|\Phi_1^-\rangle$ and $|\Phi_2^+\rangle$ states, carrying the $T^\zeta = -1$ pseudospin flavour, is coupled to the one in terms of $|\Phi_3^+\rangle$ and $|\Phi_4^-\rangle$ states, carrying the opposite $T^\zeta = 1$ flavour. Similarly, sectors with different pseudospin flavours are mixed in matrix (13). Thus, one has to determine the expectation values of $\mathcal{T}^\zeta$ by a direct evaluation using the eigenstates of the Hamiltonian.

The ground state of the t_{2g} model with finite J_H is a spin triplet accompanied by a pseudospin singlet (cf table 1). Notice however that its energy $-1.2361t$ obtained for $J_H = U/4$ differs vastly from the value $E_{T_0}^{t_{2g}} = -2t$ estimated roughly from equation (17). The reason of this discrepancy is the failure of the second-order perturbation theory controlled by $t^2/(U - 3J_H)$, being here of order $\mathcal{O}(t)$. Therefore, it can be used only for qualitative arguments in this regime, while it works better for smaller $J_H = U/8$, yielding there $-0.8t$, a value much closer to the exact energy $-0.7016t$.

Table 2. The same as in table 1 but for e_g orbitals, and four representative values of Hund's exchange: $J_H = 0$, $U/8$, $U/4$, and $U/3$.

$J_H = 0$			$J_H = U/8$			$J_H = U/4$			$J_H = U/3$		
E_n/t	S_n	T_n^ζ	E_n/t	S_n	T_n^ζ	E_n/t	S_n	T_n^ζ	E_n/t	S_n	T_n^ζ
−0.4721	0	−1	−0.4784	0	−0.9985	−0.4983	0	−0.9935	−1.0	1	0.0
−0.1231	1	0	−0.1926	1	0.0	−0.4142	1	0.0		1	0.0
	1	0		1	0.0		1	0.0	−0.5204	0	−0.9877
	0	0	−0.1401	0	0.0	−0.1623	0	0.0	−0.1813	0	0.0
	0	0		0	0.0		0	0.0		0	0.0

3.3. Eigenenergies for e_g orbitals

Turning now to the e_g orbital model and recollecting the immobile $|\xi\rangle$ orbital flavour with $t_{\xi\xi} = 0$, one immediately notices two sets of two identical 2×2 subspaces spanned by the $T^\zeta = 0$ states, described by the matrices in equations (14) and (15), which readily yield two doubly degenerate singlets (cf appendix C). Diagonalizing the submatrix (12) yields the three eigenvalues given in appendix C. The first of them (C.3) corresponds to the lowest energy low-spin state. In the strong coupling regime, i.e., for $(U - J_H) \gg t$, one finds

$$E_{S_0}^{e_g} \simeq -\frac{4t^2 U}{U^2 - J_H^2}. \tag{19}$$

It has to be compared with the lowest eigenvalue of the $S^z = 1$ subspace, the lowest energy doubly degenerate spin triplet,

$$E_{T_0}^{e_g} = \frac{1}{2}\left(U - 3J_H - \sqrt{(U - 3J_H)^2 + 4t^2}\right), \tag{20}$$

obtained by the diagonalization of the matrices (10) and (11). It corresponds, as in the model with t_{2g} orbitals, to the pseudospin singlet ($T_n = 0$). In the strong coupling regime it yields the lowest high-spin energy,

$$E_{T_0}^{e_g} \simeq -\frac{t^2}{U - 3J_H}. \tag{21}$$

Note that the energy is much higher than that for the t_{2g} model, see equation (17), as only one electron is mobile.

Based on the lowest energy excitations (19) and (21) one can easily notice a striking difference between t_{2g} and e_g orbitals with respect to the ground state. Indeed, in contrast to the t_{2g} model where even infinitesimally small Hund's exchange coupling lifts the degeneracy between the lowest energy singlet and triplet excitations and stabilizes the FM spin correlation, one can expect that the singlet state with the energy $E_{S_0}^{e_g}$ (C.3) remains the e_g ground state up to $J_H \sim U/4$.

The corresponding exact eigenenergies of the Hamiltonian (1) with e_g orbitals obtained in the strong coupling regime $U = 8t$ for a few values of J_H are listed in table 2. The data show that increasing J_H diminishes the energy difference between the lowest singlet and the first two triplet excited states. Remarkably, however, even for unrealistically large $J_H = U/4$, the e_g ground state is still a singlet with almost fully occupied mobile pseudospin $|\zeta\rangle$ orbitals (cf table 2) contradicting our predictions from the strong coupling regime. It follows from the approximate low-spin state energy $E_{S_0}^{e_g}$ (19) which overestimates the tendency towards ferromagnetism due to the performed expansion, and the transition from the singlet to the high-spin state occurs only for $J_H \simeq 0.27U$. Indeed, the ground state found for $J_H = U/3$ is a triplet, with the energy well below that of the singlet state (see table 2). Therefore, although

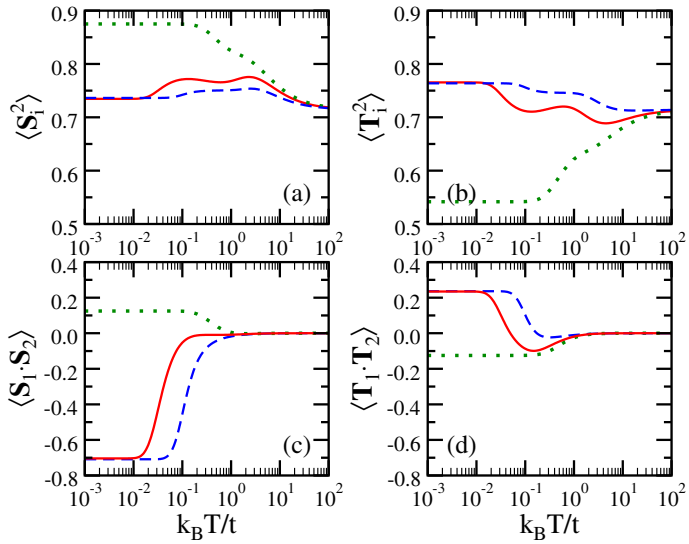

Figure 2. Temperature dependence of local moments (a) spin $\langle \mathbf{S}_i^2 \rangle$, (b) pseudospin $\langle \mathbf{T}_i^2 \rangle$, and of intersite correlations (c) spin $\langle \mathbf{S}_1 \cdot \mathbf{S}_2 \rangle$, (d) pseudospin $\langle \mathbf{T}_1 \cdot \mathbf{T}_2 \rangle$, as obtained for the model with e_g orbitals, for increasing values of Hund's exchange: $J_H = U/8$ (dashed line), $J_H = U/4$ (solid line) and $J_H = U/3$ (dotted line). Parameters: $U = 8t$, $E_0 = 0$.

Hund's exchange coupling J_H is a driving force of the FM spin correlations in both models, it is decisively more efficient in the case of t_{2g} orbitals, where already infinitesimal J_H stabilizes the high-spin state as both pseudospins are mobile.

Actually, one can rewrite the interaction term of the Hamiltonian H_{int} (6) as a superposition of interactions in different channels, involving the density, magnetization, orbital polarization, magnetic orbital polarization, and on-site orbital flip term, respectively [32]. In each of them the interaction strength is different: it is systematically attractive (repulsive) in the magnetic (density) channels, while it turns repulsive in the orbital polarization channel for $5J_H > U$. As a result, one expects a transition in the ground state from pseudospin triplet to pseudospin singlet with increasing J_H/U. This is precisely the transition we discussed above for e_g electrons. In contrast, the magnetic instability takes over for t_{2g} electrons, and the spin triplet ground state is found at any $J_H > 0$.

3.4. Correlation functions and susceptibility at orbital degeneracy

We now turn to the temperature dependence of the on-site $\langle \mathbf{S}_i^2 \rangle$ and intersite $\langle \mathbf{S}_1 \cdot \mathbf{S}_2 \rangle$ spin correlations, and the on-site $\langle \mathbf{T}_i^2 \rangle$ and intersite $\langle \mathbf{T}_1 \cdot \mathbf{T}_2 \rangle$ pseudospin correlations. The latter yield information about an orbital state together with orbital correlation between neighbouring sites.

In figure 2 we present the temperature dependence of the spin and pseudospin correlation functions as well as both susceptibilities of the model with e_g orbitals. We have set Hund's exchange coupling to be $J_H/U = 1/8$ (dashed line) and $J_H/U = 1/4$ (solid line). At low temperature, one expects charge localization as the system is in the strong coupling regime $U = 8t$. Indeed, the local spin moment $\langle \mathbf{S}_i^2 \rangle$ reaches virtually the magnitude $S(S+1) = 3/4$ for the spin $S = 1/2$. A rise of $\langle \mathbf{S}_i^2 \rangle$ above this value upon increasing temperature is caused by thermal excitations to triplet states. They are favoured by Hund's interaction and form local high-spin configurations. Consequently, the increase of $\langle \mathbf{S}_i^2 \rangle$ is larger for stronger $J_H = U/4$.

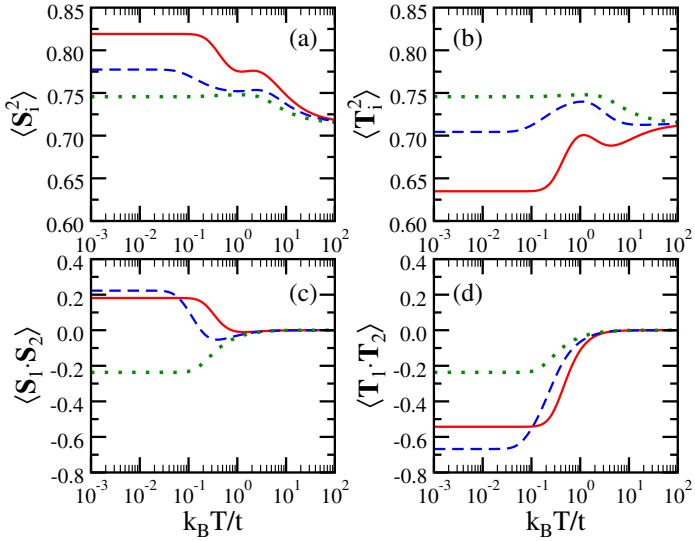

Figure 3. The same as in figure 2 but for the model with two degenerate t_{2g} orbitals, and for $J_H = 0$ (dotted line), $J_H = U/8$ (dashed line), $J_H = U/4$ (solid line).

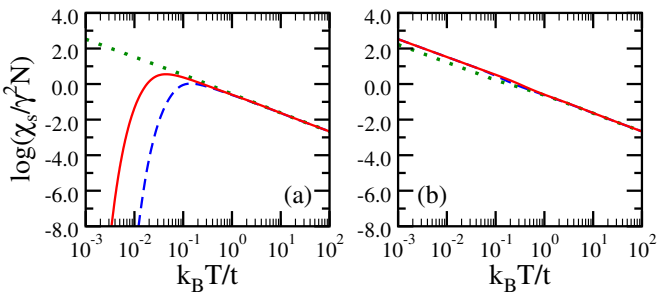

Figure 4. Temperature dependence of the spin susceptibility $\log(\chi_s/\gamma^2 N)$ per site ($N = 2$) as obtained for two values of Hund's exchange, $J_H = U/8$ (dashed lines) and $J_H = U/4$ (solid lines), for (a) e_g model, and (b) t_{2g} model. For comparison the susceptibilities obtained with $J_H = U/3$ for the e_g model and with $J_H = 0$ for the t_{2g} model are shown by dotted lines. Parameters: $U = 8t$, $E_0 = 0$.

Next, the intersite spin correlation function $\langle \mathbf{S}_1 \cdot \mathbf{S}_2 \rangle$ indicates the low-spin (AF) nature of the ground state, whereas the corresponding pseudospin function $\langle \mathbf{T}_1 \cdot \mathbf{T}_2 \rangle$ illustrates the ferro orbital (FO) pseudospin correlation.

The results obtained within the t_{2g} model are qualitatively different. First, at $J_H = 0$, apart from spin $SU(2)$ symmetry there is an additional $SU(2)$ symmetry for orbital degrees of freedom, resulting in higher $SU(4)$ symmetry [43], and the intersite spin and pseudospin correlation functions are both negative and identical. Second, at finite J_H positive $\langle \mathbf{S}_1 \cdot \mathbf{S}_2 \rangle$ indicates the FM nature of the ground state supported by the pseudospin singlet with negative $\langle \mathbf{T}_1 \cdot \mathbf{T}_2 \rangle$ correlations shown in figure 3.

The gradual increase of triplet intersite correlations $\langle \mathbf{S}_1 \cdot \mathbf{S}_2 \rangle$ observed for the e_g model is also well recognized in the spin susceptibility; see figure 4(a). Upon taking the logarithm of χ_s we find a typical AF behaviour with a characteristic cusp at the crossover temperature

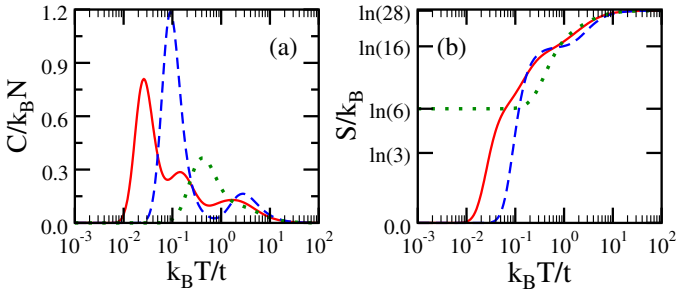

Figure 5. Temperature dependence of (a) the specific heat C per site and (b) the entropy S, as obtained for e_g orbitals with: $J_H = U/8$ (dashed line), $J_H = U/4$ (solid line), and $J_H = U/3$ (dotted line). Parameters: $U = 8t$, $E_0 = 0$.

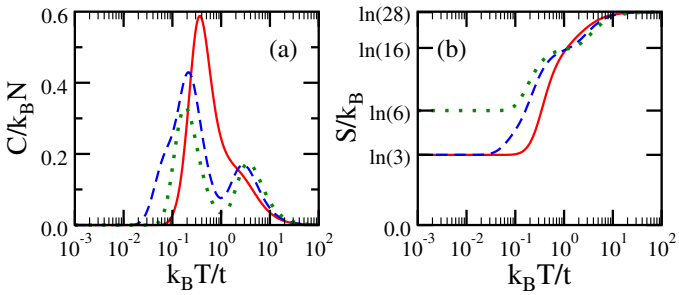

Figure 6. The same as in figure 5 but for t_{2g} orbitals. Dotted, dashed, and solid line corresponds to $J_H = 0$, $J_H = U/8$, and $J_H = U/4$, respectively.

$T_c(e_g)$. Obviously, the AF array that sets in has zero net magnetic moment at a temperature below $T_c(e_g)$ and this explains the observed cusp in χ_s. Only for large $J_H = U/3$ is the ground state a triplet, and the spin susceptibility changes to the Curie–Weiss type. In contrast, in the case of the t_{2g} model (figure 4(b)), χ_s is already large at low temperature for $J_H = 0$ as the ground state has degenerate singlet and triplet states. Increasing J_H gives here only moderate enhancement of the spin susceptibility as the degeneracy of the ground state is then removed.

3.5. Specific heat and entropy at orbital degeneracy

Different energy spectra of the e_g and t_{2g} systems result in quite different temperature behaviour of the specific heat C and the entropy S, as shown in figures 5 and 6. Consider first the e_g system. As depicted in figure 5, a low-temperature peak of the specific heat coincides with the characteristic kink in the susceptibility χ_s (cf figure 4(a)). Comparing the position of the low temperature peaks corresponding to $J_H = U/8$ and $J_H = U/4$, one finds that increasing J_H reduces the value of the characteristic temperature $T_c(e_g)$ that marks the crossover to the high-spin state for the e_g system. Note, however, that for $J_H = U/4$ the low-temperature peak in the specific heat splits into two. The first one corresponds to a transition from the singlet ground state to the first two triplet excited states with the excitation energy $\Delta E_1/t = 0.0841$, whereas the second one appears due to the higher energy charge excitations, with the excitation energies $\Delta E_2/t = 0.336$ and $\Delta E_3/t = 0.498$, respectively. In contrast, when $J_H = U/8$ the excitation energy into the first excited state is much larger, $\Delta E_1'/t = 0.286$, whereas the other excitation

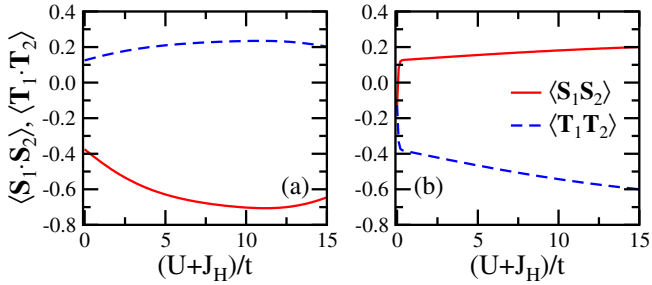

Figure 7. Zero temperature intersite correlation functions: spin $\langle \mathbf{S}_1 \cdot \mathbf{S}_2 \rangle$ (solid lines) and pseudospin $\langle \mathbf{T}_1 \cdot \mathbf{T}_2 \rangle$ (dashed lines) as functions of the Stoner parameter $U + J_{\mathrm{H}}$ in the two-band model at $J_{\mathrm{H}} = U/4$ for (a) $\mathrm{e_g}$ orbitals, and (b) $\mathrm{t_{2g}}$ orbitals.

energies are nearly unaltered: $\Delta E_2'/t = 0.338$ and $\Delta E_3'/t = 0.478$. This results in a single broad low-temperature peak. High-temperature peaks occur due to thermal excitations which create double occupancies and lead to charge delocalization, well seen in the suppression of $\langle \mathbf{S}_i^2 \rangle$. Finally, at large $J_{\mathrm{H}} = U/3$ all peaks in the specific heat merge into a single broad peak at higher temperature.

Turning now to the temperature dependence of the entropy depicted in figure 5(b), one finds $S \simeq 0$ in the low-T regime for the singlet ground state. Basically, the overall rapid increase of the entropy around $T_{\mathrm{c}}(\mathrm{e_g})$ in figure 5(b) is very much the same for $J_{\mathrm{H}} = U/8$ and $J_{\mathrm{H}} = U/4$, corresponding to the low-temperature peak in the specific heat. However, a detailed behaviour of S depends on J_{H}. In the regime of small Hund's exchange $J_{\mathrm{H}} \leqslant U/8$, where $L_S = 16$ singly occupied states are well separated from doubly occupied ones, S possesses a point of inflection $S = k_{\mathrm{B}} \ln 16$ at $k_{\mathrm{B}} T \simeq t$, which follows from the gapped character of the specific heat. In contrast, for the larger $J_{\mathrm{H}} = U/4$, the entropy increase starts at lower temperature as the energy of the singlet–triplet excitation is low. Here the gap between singly and doubly occupied states is smaller and the corresponding point of inflection is less transparent. The limiting value $S = k_{\mathrm{B}} \ln 28$ results from the calculation performed in the canonical ensemble.

The situation is quite different in the case of the $\mathrm{t_{2g}}$ model. Unlike the $\mathrm{e_g}$ case, increasing J_{H} shifts $T_{\mathrm{c}}(\mathrm{t_{2g}})$ towards higher temperatures (figure 6). As a result, the crossover temperatures of both systems differ substantially, especially in the regime of large Hund's exchange coupling $J_{\mathrm{H}} \sim U/4$. Indeed, from the position of the low-temperature peak of the specific heat in figures 5(a) and 6(a), one can read off that $k_{\mathrm{B}} T_{\mathrm{c}}(\mathrm{e_g}) = 0.025t$, whereas $k_{\mathrm{B}} T_{\mathrm{c}}(\mathrm{t_{2g}}) = 0.35t$. The origin of this marked difference is certainly the fact that increasing J_{H} diminishes (enlarges) the gap between the spin singlet (triplet) ground state and the first excited triplet (singlet) state of the $\mathrm{e_g}$ ($\mathrm{t_{2g}}$) system, respectively (cf tables 1 and 2). In contrast to the $\mathrm{e_g}$ case, the entropy is finite in the low-temperature regime, and approaches either the value $k_{\mathrm{B}} \ln 3$ for both $J_{\mathrm{H}} = U/8$ and $J_{\mathrm{H}} = U/4$ or $k_{\mathrm{B}} \ln 6$ when $J_{\mathrm{H}} = 0$; see figure 6(b). Indeed, for $J_{\mathrm{H}} = 0$, the ground state corresponds to six degenerate states—three of them constitute a spin triplet, whereas the others are singlets, as shown in table 1. However, any finite $J_{\mathrm{H}} > 0$ splits up these states and leads to the triplet ground state with the entropy $S = k_{\mathrm{B}} \ln 3$. As in the $\mathrm{e_g}$ case, S has a clear point of inflection only in the regime of small Hund's exchange coupling $J_{\mathrm{H}} \leqslant U/8$.

To summarize this section, we compare in figure 7 the intersite spin $\langle \mathbf{S}_1 \cdot \mathbf{S}_2 \rangle$ and pseudospin $\langle \mathbf{T}_1 \cdot \mathbf{T}_2 \rangle$ correlation functions for the $\mathrm{e_g}$ system (cf figure 7(a)) and for the $\mathrm{t_{2g}}$ system (cf figure 7(b)) as a functions of the Stoner parameter $U + J_{\mathrm{H}}$. Note that $\langle \mathbf{S}_1 \cdot \mathbf{S}_2 \rangle$ is finite and negative even in the noninteracting $U = 0$ limit due to the Pauli principle. On the

one hand, the e_g results illustrate the AF correlations in the ground state (negative $\langle \mathbf{S}_1 \cdot \mathbf{S}_2 \rangle$) owing to the preferred mobile pseudospin $|\zeta\rangle$. On the other hand, the ground state of the t_{2g} system with a finite interaction is a spin triplet as $\langle \mathbf{S}_1 \cdot \mathbf{S}_2 \rangle$ is positive and a pseudospin singlet as the corresponding correlation function $\langle \mathbf{T}_1 \cdot \mathbf{T}_2 \rangle$ is negative. We therefore conclude that the ground state properties strongly depend on the orbital correlations, in agreement with the Goodenough–Kanamori rules [34].

4. New features at finite crystal field

4.1. Correlation functions and susceptibility at finite crystal field

We now discuss the influence of the crystal field splitting given by equation (7). Here we are interested in the nontrivial case of crystal field acting along the c axis *perpendicular* to the chain. Hence, as we have been working with the e_g orbital basis consisting of a directional orbital along the molecular bond $|\zeta\rangle$ and an orthogonal to it planar orbital $|\xi\rangle$, one needs to rotate the field (7) expressed in the original orbital basis $\{|x\rangle, |z\rangle\}$ by the same angle $\theta = 2\pi/3$ which enabled us to simplify the form of the hopping matrix (2) into (4). Making the inverse transformation to (3) in equation (7), one obtains the crystal field term,

$$H_{\mathrm{cf}} = \tfrac{1}{2} E_0 \sum_{i\sigma} \left[\cos\theta (c^{\dagger}_{i\xi\sigma} c_{i\xi\sigma} - c^{\dagger}_{i\zeta\sigma} c_{i\zeta\sigma}) + \sin\theta (c^{\dagger}_{i\xi\sigma} c_{i\zeta\sigma} + c^{\dagger}_{i\zeta\sigma} c_{i\xi\sigma}) \right]. \tag{22}$$

Note that $\cos\theta$ is negative so the field (22) favours the $|\xi\rangle$ occupancy over the $|\zeta\rangle$ occupancy, as it should.

Unfortunately, except for the Hamiltonian matrix (11), the form of the other matrices is now considerably more involved due to off-diagonal elements in the crystal field in equation (22) which couple states with different T^{ζ}. In general, it is not possible to obtain analytic expressions for the eigenvalues and one has to resort to a numerical diagonalization. However, due to the equivalent hopping amplitudes, the eigenvalues of the t_{2g} model should be independent of the rotation angle θ, i.e., one has to get the same energy spectrum for the field (22) with finite θ, as well as for the diagonal in pseudospin space field of the form $E_0 \mathcal{T}^{\zeta}$. This latter field acts along the chain and corresponds to $\theta = 0$ in equation (22).

Numerical values of the eigenvalues obtained for t_{2g} orbitals for $E_0 = 2t$ and $\theta = 2\pi/3$ are listed in table 3. Although the energy spectrum of the t_{2g} model indeed does not depend on the field direction, expectation values of $\mathcal{T}^{\zeta}$ in the Hamiltonian eigenstates certainly do, as a finite rotation angle θ enables the mixing of states with different values of $\mathcal{T}^{\zeta}$. For example, the initial pseudospin $T^{\zeta} = \pm 1$ of spin triplets with the energy $E_0/t = \pm 2$ is reduced up to $T^{\zeta} = \pm 0.5$ by the field with $\theta = 2\pi/3$ (cf table 3), whereas it is conserved when $\theta = 0$.

Contrary to the $E_0 = 0$ case with a spin triplet and pseudospin singlet as the t_{2g} ground state at finite $J_{\mathrm{H}} > 0$, finite positive E_0 suppresses the AO pseudospin correlation and stabilizes a spin singlet with a positive value of $T^{\zeta} \simeq 0.5$, inducing FO correlations. Remarkably, the effect of the crystal field on the e_g ground state is just the opposite, as reported in table 4. Namely, by lifting the degeneracy of pseudospin flavours it promotes the immobile $|\xi\rangle$ one. Consequently, there is not that much kinetic energy to be gained and the Coulomb interactions start to be crucial. However, they are noticeably better optimized by the FM spin correlation. Indeed, from table 4 one sees a strong competition between the lowest singlet and triplet states, both with a positive (but still smaller than in the t_{2g} case) value of $T^{\zeta} \simeq 0.45$. Note also that it becomes energetically advantageous to have the spin triplet as the ground state for large $J_{\mathrm{H}} = U/4$ while a smaller Hund's exchange coupling $J_{\mathrm{H}} = U/8$ drives the system towards the singlet in the ground state.

Table 3. Eigenenergies of model (1) with t_{2g} orbitals as obtained at $U = 8t$ with a finite crystal field $E_0 = 2t$ acting perpendicular to the chain, for two values of Hund's exchange: $J_H = U/8$ and $J_H = U/4$. The spin quantum number S_n and the expectation value of T_n^ζ operator (9) in each eigenstate $|n\rangle$ are given.

$J_H = U/8$			$J_H = U/4$		
E_n/t	S_n	T_n^ζ	E_n/t	S_n	T_n^ζ
−2.4767	0	0.4995	−2.4910	0	0.4980
−2.0	1	0.5	−2.0	1	0.5
−0.7016	1	0.0	−1.2361	1	0.0
−0.5311	0	0.0	−0.6056	0	0.0
0.0	1	0.0	0.0	1	0.0
	0	0.0		0	0.0
1.5183	0	−0.4977	1.4876	0	−0.4899
2.0	1	−0.5	2.0	1	−0.5
5.0	1	0.0		1	0.0
5.7016	1	0.0	3.2361	1	0.0
5.7639	0	0.4472	5.1716	0	0.3536
6.2695	0	0.4498	5.7610	0	0.3539
7.0	0	0.0	6.0	0	0.0
7.5311	0	0.0	6.6056	0	0.0
10.2361	0	−0.4472	10.8284	0	−0.3536
10.6890	0	−0.4516	11.2424	0	−0.3620

Table 4. The same as in table 3 but for e_g orbitals.

$J_H = U/8$			$J_H = U/4$		
E_n/t	S_n	T_n^ζ	E_n/t	S_n	T_n^ζ
−2.0786	0	0.4229	−2.0965	1	0.4429
−2.0548	1	0.4695	−2.0852	0	0.4179
−0.2286	0	−0.0348	−0.4142	1	0.0
−0.1926	1	0.0	−0.2410	0	−0.0305
−0.1468	0	0.0002	−0.1703	0	0.0003
−0.0494	1	0.0734	−0.1169	1	0.1658
1.6727	0	−0.3841	1.5089	1	−0.4969
1.8878	1	−0.5409	1.6340	0	−0.3713
5.1926	1	0.0	2.4142	1	0.0
5.2165	1	−0.0020	2.7045	1	−0.1118
5.8526	0	0.4929	5.2848	0	0.4140
5.8564	0	0.4885	5.3156	0	0.3627
7.0374	0	−0.0538	6.0468	0	−0.0631
7.2305	0	0.0461	6.2702	0	0.0517
10.2567	0	−0.4394	10.8387	0	−0.3512
10.5476	0	−0.5385	11.1064	0	−0.4305

4.2. Specific heat and entropy at finite crystal field

The above ground states and the excitation spectra obtained at finite crystal field $E_0 = 2t$ influence the intersite spin and orbital correlations, shown in figure 8. The ground state of the e_g system depends on the value of J_H, being a spin singlet for $J_H = U/8$ which results in negative $\langle \mathbf{S}_1 \cdot \mathbf{S}_2 \rangle$ and a spin triplet for $J_H = U/4$ yielding positive $\langle \mathbf{S}_1 \cdot \mathbf{S}_2 \rangle$ in the low-temperature regime. In contrast, $\langle \mathbf{T}_1 \cdot \mathbf{T}_2 \rangle$ is positive (FO pseudospin correlations) and almost insensitive

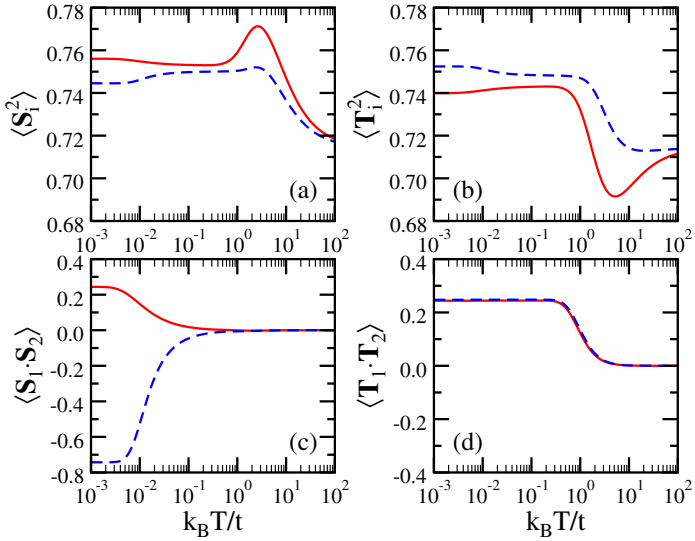

Figure 8. Temperature dependence of local moments (a) spin $\langle \mathbf{S}_i^2 \rangle$ and (b) pseudospin $\langle \mathbf{T}_i^2 \rangle$, and of intersite correlation functions (c) spin $\langle \mathbf{S}_1 \cdot \mathbf{S}_2 \rangle$ and (d) pseudospin $\langle \mathbf{T}_1 \cdot \mathbf{T}_2 \rangle$, as obtained for the model with e_g orbitals for $J_H = U/8$ (dashed lines) and $J_H = U/4$ (solid lines). Parameters: $U = 8t$ and $E_0 = 2t$.

to the value of J_H at low temperature. For increasing temperature one finds two transitions—first, the intersite spin correlations weaken, and second, the pseudospin correlations weaken at much higher temperature, when charge excitations are thermally activated. This separation of the energy scales for spin and orbital excitations occurs both for lower $J_H = U/8$ and higher $J_H = U/4$.

A finite crystal field drastically affects the behaviour of the t_{2g} correlation functions as well (figure 9). At low temperature, negative $\langle \mathbf{S}_1 \cdot \mathbf{S}_2 \rangle$ reveals the AF coupling between spins, whereas positive $\langle \mathbf{T}_1 \cdot \mathbf{T}_2 \rangle$ indicates the FO pseudospin correlation, regardless of J_H. In contrast to the e_g case, however, spin and pseudospin correlations are reduced and vanish simultaneously, indicating that spin–orbital degrees of freedom are coupled more strongly in this case [21].

The change of the magnetic correlations with increasing J_H in the e_g model is reflected in the crossover from the AF behaviour of χ_s at $J_H = U/8$ to the Curie–Weiss behaviour of χ_s obtained for $J_H = U/4$; see figure 10(a). In the case of the t_{2g} model (figure 10(b)) one finds the AF character of χ_s in the interesting range of J_H. Altogether, as for $E_z = 0$, the spin susceptibility χ_s exhibits again the opposite behaviour for both types of orbital—the high-spin state is suppressed in the t_{2g} model, while it can be selected by the crystal field in the e_g model. The maximum of χ_s occurs at higher temperature in t_{2g} than in e_g model at $J_H = U/8$.

4.3. Specific heat and entropy

As expected from the above results, a finite crystal field also modifies the temperature evolution of the specific heat C and the entropy S for e_g orbitals; see figure 11. The position of the high-temperature peak of the specific heat at $k_B T \simeq t$ is almost the same as the position of the strong anomalies of both on-site correlation functions (cf figures 11(a) and 8). Depending on J_H, the low-temperature entropy S of the e_g system either vanishes (for the singlet ground state

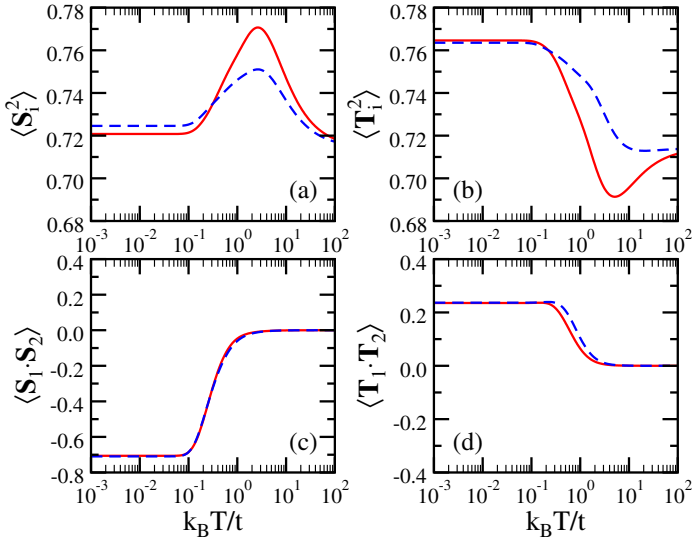

Figure 9. The same as in figure 8 but for the model with t_{2g} orbitals. The dashed (solid) line corresponds to $J_H = U/8$ ($J_H = U/4$), respectively.

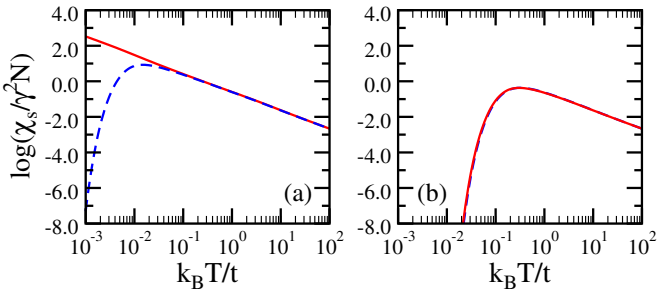

Figure 10. Temperature dependence of the spin susceptibility $\log(\chi_s/\gamma^2 N)$ per site ($N = 2$) for (a) e_g model, and (b) t_{2g} model, as obtained for two values of Hund's exchange: $J_H = U/8$ (dashed lines) and $J_H = U/4$ (solid lines). Parameters: $U = 8t$, $E_0 = 2t$.

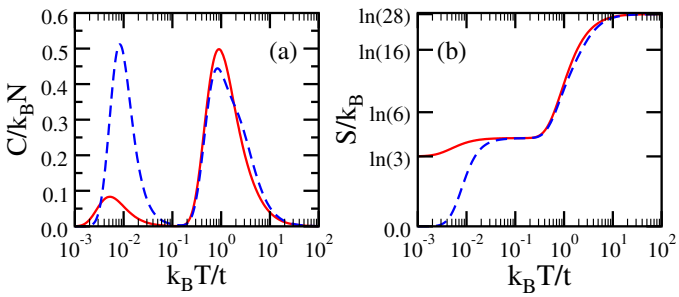

Figure 11. Temperature dependence of: (a) the specific heat C, and (b) the entropy S for e_g orbitals. The dashed (solid) line corresponds to $J_H = U/8$ ($J_H = U/4$), respectively. Parameters: $U = 8t$ and $E_0 = 2t$.

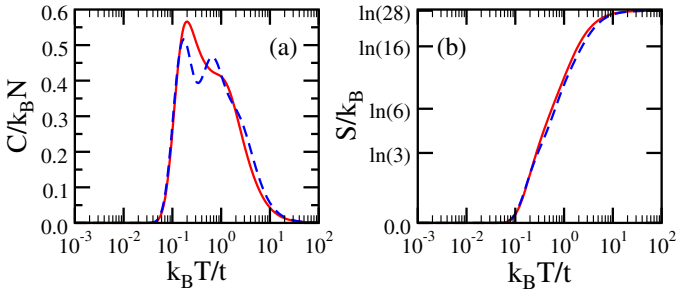

Figure 12. The same as in figure 11 but for t_{2g} orbitals. The dashed (solid) line corresponds to $J_H = U/8$ ($J_H = U/4$), respectively.

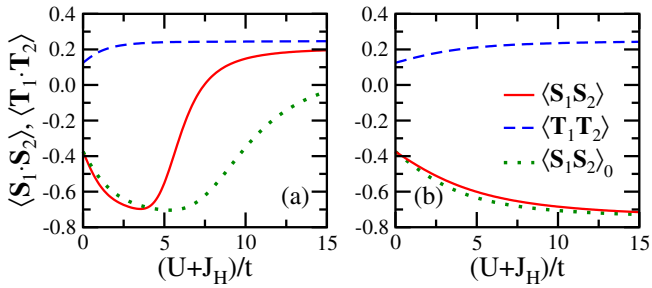

Figure 13. Zero temperature intersite correlation functions: spin $\langle \mathbf{S}_1 \cdot \mathbf{S}_2 \rangle$ (solid lines) and pseudospin $\langle \mathbf{T}_1 \cdot \mathbf{T}_2 \rangle$ (dashed lines) as functions of the Stoner parameter $U + J_H$ for (a) e_g orbitals, and (b) t_{2g} orbitals. Parameters: $E_0 = 2t$, $J_H = U/4$. The dotted line shows the spin–spin correlation function $\langle \mathbf{S}_1 \cdot \mathbf{S}_2 \rangle_0$ obtained in the Ising limit (see text).

as $J_H \leqslant U/8$) or approaches the value $k_B \ln 3$ (for the triplet ground state at $J_H = U/4$). Nevertheless, owing to the vanishing specific heat, all the curves in figure 11(b) have a point of inflection $S = k_B \ln 4$ at $k_B T \simeq 0.1t$. Note that in contrast to the case without a crystal field, there is no such a point when $S = k_B \ln 16$. Namely, by promoting one pseudospin over the other one, a finite crystal field markedly lowers the states with double occupancies; hence the usual gap between the singly and doubly occupied states vanishes.

Consider now the temperature behaviour of the specific heat for t_{2g} orbitals shown in figure 12(a). Instead of the high- and low-temperature peaks of the specific heat one observes two slightly separated peaks for $J_H = U/8$ which merge into a wide peak at $J_H = U/4$. This confirms that spin–orbital degrees of freedom are strongly coupled as spin and orbital intersite correlations change at the same temperature (see figure 9). Finally, as shown in figure 12(b), the entropy of the t_{2g} system is almost independent of J_H. We note that S is entirely suppressed at low T due to a spin singlet ground state; it rises rapidly at $k_B T \simeq 0.1t$, and eventually approaches the limiting value $S = k_B \ln 28$, not having any point of inflection. Such a behaviour is a direct consequence of a single broad peak in the specific heat and no separation of the energy scales for spin and orbital excitations.

We close this section with a short discussion of the intersite spin $\langle \mathbf{S}_1 \cdot \mathbf{S}_2 \rangle$ and pseudospin $\langle \mathbf{T}_1 \cdot \mathbf{T}_2 \rangle$ correlations for the e_g system depicted in figure 13(a) as functions of the Stoner parameter, $I = U + J_H$, in the presence of a finite crystal field $E_0 = 2t$. As expected, the results illustrate the AF correlation between spins on two sites in the weak coupling regime

$U + J_{\rm H} \lesssim 7t$. However, further increase of the interaction strength gradually changes the AF coupling into an FM one, with the immobile $|\xi\rangle$ pseudospin component preferred by the crystal field. Remarkably, such a transition at $U + J_{\rm H} \simeq 16t$ in the presence of the same crystal field $E_0 = 2t$ from the AF phase into the FM one has been obtained on the infinite lattice in the Hartree approximation recently [33]. (The mean field phase diagram appears more involved [32], since FM order is stabilized for $5 \leqslant I/t \leqslant 6.5$, in contrast to what is obtained in the present study. Nevertheless this mostly reflects the strong competition between the FM and AF phases, since their energy does not differ by more than 1% in this regime [44].) Consequently, owing to a strong competition between the singlet and triplet states with the lowest energies (cf table 4), respectively, one can conjecture that fluctuations clearly affect the intersite spin correlations. Indeed, comparison of $\langle \mathbf{S}_1 \cdot \mathbf{S}_2 \rangle$ and $\langle \mathbf{S}_1 \cdot \mathbf{S}_2 \rangle_0$ determined in the Ising limit (i.e., taking only S_i^z operators and neglecting the last term in the Hamiltonian (6)) shows that dynamics acts to reduce the AF coupling between spins. In contrast, a finite crystal field affects $\langle \mathbf{T}_1 \cdot \mathbf{T}_2 \rangle$ only slightly, and the pseudospin correlations are always positive for increasing I regardless of E_0, which implies the FO coupling between two pseudospins (cf figures 7(a) and 13(a)). Thus, in the regime of large Stoner parameter I one finds that the classical Goodenough–Kanamori rules [34] are violated as the crystal field stabilizes a particular orbital configuration. In contrast to quantum spin–orbital entanglement [35], this effect here is static and may play an important role for the observed magnetic and orbital correlations in transition metal oxides, as discussed recently on the example of $LiNiO_2$ [45].

Turning now to the t_{2g} model with positive $\langle \mathbf{S}_1 \cdot \mathbf{S}_2 \rangle$ and negative $\langle \mathbf{T}_1 \cdot \mathbf{T}_2 \rangle$ in the degenerate case shown in figure 7(b), the situation is also changed drastically by a finite crystal field as depicted in figure 13(b). Indeed, the resulting $\langle \mathbf{S}_1 \cdot \mathbf{S}_2 \rangle$ is then negative, revealing the AF nature of the ground state. However, due to the energy gap between a singlet ground state and the first excited triplet state (cf table 3), the fluctuations modify the value of the intersite spin correlations only slightly, so $\langle \mathbf{S}_1 \cdot \mathbf{S}_2 \rangle$ and $\langle \mathbf{S}_1 \cdot \mathbf{S}_2 \rangle_0$ almost overlap. Finally, positive $\langle \mathbf{T}_1 \cdot \mathbf{T}_2 \rangle$ shows that the AO pseudospin correlations found before at $E_0 = 0$ are suppressed.

5. Summary

We have obtained the exact numerical results for a two-site Hubbard model with two e_g orbitals at quarter-filling. By an appropriate transformation of the original orbital basis $\{|x\rangle, |z\rangle\}$ into a basis consisting of a directional orbital $|\zeta\rangle$ along the molecular bond and a planar and orthogonal to it orbital $|\xi\rangle$, we have simplified the hopping matrix, making use of the properties of e_g orbitals—the electrons in $|\zeta\rangle$ directional orbitals are mobile, while those in orthogonal $|\xi\rangle$ orbitals are fully localized [38]. The results were compared with the doubly degenerate Hubbard model with two equivalent t_{2g} orbitals active along the molecular bond direction.

As the first important result, a striking difference between t_{2g} and e_g orbitals with respect to the ground state has been established. Indeed, in contrast to the t_{2g} model, where even infinitesimally small Hund's exchange $J_{\rm H} > 0$ lifts the degeneracy of the lowest energy singlet and triplet states and stabilizes the FM spin correlation, we have found that a spin singlet ground state survives up to $J_{\rm H} \simeq 0.27U$ for e_g electrons. In this regime of parameters, the intersite spin correlations $\langle \mathbf{S}_1 \cdot \mathbf{S}_2 \rangle$ indicate the AF nature of the ground state, whereas the pseudospin function $\langle \mathbf{T}_1 \cdot \mathbf{T}_2 \rangle$ illustrates the FO pseudospin correlation. On the contrary, in the t_{2g} model, except for $J_{\rm H} = 0$ when the intersite spin and pseudospin correlation functions overlap and are negative, positive $\langle \mathbf{S}_1 \cdot \mathbf{S}_2 \rangle$ demonstrates the FM nature of the ground state supported by the pseudospin singlet with negative $\langle \mathbf{T}_1 \cdot \mathbf{T}_2 \rangle$, i.e., AO correlations. Therefore, a complementary behaviour of the spin and orbital flavours is observed as a generic feature of both models, in agreement with the Goodenough–Kanamori rules [34].

We have further demonstrated the influence of a finite crystal field E_0 on the ground state. On the one hand, it suppresses the FM spin correlation in the t_{2g} model and stabilizes the spin singlet ground state with negative $\langle \mathbf{S}_1 \cdot \mathbf{S}_2 \rangle$, accompanied by positive $\langle \mathbf{T}_1 \cdot \mathbf{T}_2 \rangle$. On the other hand, the effect of the crystal field on the e_g ground state is the opposite one. Namely, by lifting the degeneracy of the pseudospin flavours it promotes the immobile $|\xi\rangle$ one. Consequently, not much kinetic energy can be gained and the Coulomb interactions start to dominate. However, they are noticeably better optimized by the FM spin correlation. Therefore, it becomes energetically advantageous to have the spin triplet, and the ground state for large $J_H = U/4$ yields positive $\langle \mathbf{S}_1 \cdot \mathbf{S}_2 \rangle$, while a smaller Hund's exchange coupling $J_H = U/8$ drives the system towards the singlet in the ground state which results in negative $\langle \mathbf{S}_1 \cdot \mathbf{S}_2 \rangle$. In contrast, $\langle \mathbf{T}_1 \cdot \mathbf{T}_2 \rangle$ is positive and almost insensitive to the actual value of J_H in the range $0 < J_H < U/4$.

Next, we have investigated how the e_g ground state properties evolve as a function of the Stoner parameter $I = U + J_H$ in the presence of a finite crystal field $E_0 = 2t$. As expected, we have found the AF correlation between spins on two sites in the weak coupling regime $U + J_H \lesssim 7t$. However, further increase of the interaction strength gradually changes the AF coupling into an FM one, with an immobile $|\xi\rangle$ pseudospin, preferred by the crystal field. Finally, by comparing the correlation function $\langle \mathbf{S}_1 \cdot \mathbf{S}_2 \rangle$ with the one determined in the Ising limit $\langle \mathbf{S}_1 \cdot \mathbf{S}_2 \rangle_0$, we have elucidated the role of fluctuations in the intersite spin correlation function and have observed that the dynamics helps to reduce strongly the AF coupling between spins in this case. In contrast, when the ground state is FM, fluctuations only slightly modify the value of the intersite spin correlations, so $\langle \mathbf{S}_1 \cdot \mathbf{S}_2 \rangle$ and $\langle \mathbf{S}_1 \cdot \mathbf{S}_2 \rangle_0$ almost overlap.

Although our results presented here are only a starting point and a systematic analysis of the properties of the ground states and spin–orbital correlations in realistic two-band models with e_g and t_{2g} orbitals of higher dimension is required, our study shows that the description of transition metal oxides with partly filled (almost) degenerate orbitals has to involve correct symmetry of the orbital degrees of freedom, and thus has to go beyond the simplified Hubbard model with degenerate equivalent orbitals. This observation is also supported by our recent study of stripe phases in the nickelates [46]. Indeed, the diagonal stripe structures with filling of nearly one hole per atom in a domain wall, as observed experimentally, are the ground state of the model with the physically relevant hopping elements between e_g orbitals, while instead the most stable stripes have half-filled domain wall atoms within the doubly degenerate Hubbard model. We therefore conclude that the ground state properties strongly depend on the orbital degrees of freedom that are active in a given compound.

Acknowledgments

We thank C Lacroix and V Caignaert for valuable and encouraging discussions. M Raczkowski acknowledges support from the European Community under Marie Curie Program number HPMT2000-141. This work was supported by the Polish Ministry of Science and Education, Project No 1 P03B 068 26, and by the Ministère Français des Affaires Etrangères under POLONIUM 09294VH.

Appendix A. Construction of the basis for the two-site model

We construct a basis of the Hilbert space, starting with the $S^z = 1$ subspace. There are two states with $T^\zeta = \pm 1$,

$$|\Psi_{\zeta\uparrow}\rangle = c^\dagger_{1\zeta\uparrow} c^\dagger_{2\zeta\uparrow}|0\rangle, \qquad |\Psi_{\xi\uparrow}\rangle = c^\dagger_{1\xi\uparrow} c^\dagger_{2\xi\uparrow}|0\rangle, \tag{A.1}$$

and four with $T^\zeta = 0$,

$$|\Psi^{\pm}_{1\uparrow}\rangle = \frac{1}{\sqrt{2}}(c^{\dagger}_{1\xi\uparrow}c^{\dagger}_{2\zeta\uparrow} \pm c^{\dagger}_{1\zeta\uparrow}c^{\dagger}_{2\xi\uparrow})|0\rangle, \tag{A.2}$$

$$|\Psi^{\pm}_{2\uparrow}\rangle = \frac{1}{\sqrt{2}}(c^{\dagger}_{1\xi\uparrow}c^{\dagger}_{1\zeta\uparrow} \pm c^{\dagger}_{2\xi\uparrow}c^{\dagger}_{2\zeta\uparrow})|0\rangle. \tag{A.3}$$

In the $S^z = 0$ subspace there are eight states with $T^\zeta = \pm 1$,

$$|\Phi^{\pm}_{1}\rangle = \frac{1}{\sqrt{2}}(c^{\dagger}_{1\zeta\uparrow}c^{\dagger}_{2\zeta\downarrow} \pm c^{\dagger}_{1\zeta\downarrow}c^{\dagger}_{2\zeta\uparrow})|0\rangle, \tag{A.4}$$

$$|\Phi^{\pm}_{2}\rangle = \frac{1}{\sqrt{2}}(c^{\dagger}_{1\zeta\uparrow}c^{\dagger}_{1\zeta\downarrow} \pm c^{\dagger}_{2\zeta\uparrow}c^{\dagger}_{2\zeta\downarrow})|0\rangle, \tag{A.5}$$

$$|\Phi^{\pm}_{3}\rangle = \frac{1}{\sqrt{2}}(c^{\dagger}_{1\xi\uparrow}c^{\dagger}_{1\xi\downarrow} \pm c^{\dagger}_{2\xi\uparrow}c^{\dagger}_{2\xi\downarrow})|0\rangle, \tag{A.6}$$

$$|\Phi^{\pm}_{4}\rangle = \frac{1}{\sqrt{2}}(c^{\dagger}_{1\xi\uparrow}c^{\dagger}_{2\xi\downarrow} \pm c^{\dagger}_{1\xi\downarrow}c^{\dagger}_{2\xi\uparrow})|0\rangle, \tag{A.7}$$

and eight with $T^\zeta = 0$,

$$|\Phi^{\pm}_{5}\rangle = \tfrac{1}{2}(c^{\dagger}_{1\xi\uparrow}c^{\dagger}_{1\zeta\downarrow} + c^{\dagger}_{1\xi\downarrow}c^{\dagger}_{1\zeta\uparrow} \pm (c^{\dagger}_{2\xi\uparrow}c^{\dagger}_{2\zeta\downarrow} + c^{\dagger}_{2\xi\downarrow}c^{\dagger}_{2\zeta\uparrow}))|0\rangle, \tag{A.8}$$

$$|\Phi^{\pm}_{6}\rangle = \tfrac{1}{2}(c^{\dagger}_{1\xi\uparrow}c^{\dagger}_{2\zeta\downarrow} + c^{\dagger}_{1\xi\downarrow}c^{\dagger}_{2\zeta\uparrow} \pm (c^{\dagger}_{1\zeta\downarrow}c^{\dagger}_{2\xi\uparrow} + c^{\dagger}_{1\zeta\uparrow}c^{\dagger}_{2\xi\downarrow}))|0\rangle, \tag{A.9}$$

$$|\Phi^{\pm}_{7}\rangle = \tfrac{1}{2}(c^{\dagger}_{1\xi\uparrow}c^{\dagger}_{1\zeta\downarrow} - c^{\dagger}_{1\xi\downarrow}c^{\dagger}_{1\zeta\uparrow} \pm (c^{\dagger}_{2\xi\uparrow}c^{\dagger}_{2\zeta\downarrow} - c^{\dagger}_{2\xi\downarrow}c^{\dagger}_{2\zeta\uparrow}))|0\rangle, \tag{A.10}$$

$$|\Phi^{\pm}_{8}\rangle = \tfrac{1}{2}(c^{\dagger}_{1\xi\uparrow}c^{\dagger}_{2\zeta\downarrow} - c^{\dagger}_{1\xi\downarrow}c^{\dagger}_{2\zeta\uparrow} \pm (c^{\dagger}_{1\zeta\downarrow}c^{\dagger}_{2\xi\uparrow} - c^{\dagger}_{1\zeta\uparrow}c^{\dagger}_{2\xi\downarrow}))|0\rangle. \tag{A.11}$$

The states $|\Phi^{+}_{1}\rangle$ and $|\Phi^{+}_{4}\rangle$, together with $|\Phi^{\pm}_{5}\rangle$ and $|\Phi^{\pm}_{6}\rangle$, belong to the triplet subspace.

Appendix B. Eigenvalues of the Hamiltonian (1) with t_{2g} orbitals

Below we give a complete list of the eigenvalues of Hamiltonian (1) for t_{2g} orbitals in the absence of crystal field splitting (at $E_0 = 0$) with the degeneracy of the states given in parentheses.

- $S = 1$ subspace

$$\tfrac{1}{2}\left\{U - 3J_{\mathrm{H}} \pm \sqrt{(U - 3J_{\mathrm{H}})^2 + 16t^2}\right\}(3), \qquad U - 3J_{\mathrm{H}}\ (3), \quad 0\ (9); \tag{B.1}$$

- $S = 0$ subspace

$$\tfrac{1}{2}\left\{U - J_{\mathrm{H}} \pm \sqrt{(U - J_{\mathrm{H}})^2 + 16t^2}\right\}(2), \qquad U - J_{\mathrm{H}}\ (2), \tag{B.2}$$

and

$$\tfrac{1}{2}\left\{U + J_{\mathrm{H}} \pm \sqrt{(U + J_{\mathrm{H}})^2 + 16t^2}\right\}, \qquad U + J_{\mathrm{H}}, \quad 0. \tag{B.3}$$

Appendix C. Eigenvalues of the Hamiltonian (1) with e_g orbitals

Finally we present the eigenvalues of the Hamiltonian given by equation (1) for e_g orbitals in the absence of crystal field splitting (at $E_0 = 0$). The degeneracy of the states is given in parentheses.

- $S = 1$ subspace

$$\tfrac{1}{2}\left\{U - 3J_{\mathrm{H}} \pm \sqrt{(U - 3J_{\mathrm{H}})^2 + 4t^2}\right\}(6), \qquad 0\ (6); \tag{C.1}$$

- $S = 0$ subspace

$$\tfrac{1}{2}\left\{U - J_{\mathrm{H}} \pm \sqrt{(U - J_{\mathrm{H}})^2 + 4t^2}\right\}\ (2), \qquad U \pm J_{\mathrm{H}}, \quad 0, \tag{C.2}$$

and,

$$\lambda_{-1} = \frac{2U}{3}\left\{1 - \sqrt{1 + 3\left(\frac{J_{\mathrm{H}}}{U}\right)^2 + 12\left(\frac{t}{U}\right)^2}\cos\left(\frac{\alpha}{3}\right)\right\}, \tag{C.3}$$

$$\lambda_{0} = \frac{2U}{3}\left\{1 + \sqrt{1 + 3\left(\frac{J_{\mathrm{H}}}{U}\right)^2 + 12\left(\frac{t}{U}\right)^2}\cos\left(\frac{\pi + \alpha}{3}\right)\right\}, \tag{C.4}$$

$$\lambda_{1} = \frac{2U}{3}\left\{1 + \sqrt{1 + 3\left(\frac{J_{\mathrm{H}}}{U}\right)^2 + 12\left(\frac{t}{U}\right)^2}\cos\left(\frac{\pi - \alpha}{3}\right)\right\}, \tag{C.5}$$

with

$$\cos(\alpha) = \frac{1 - (\frac{3J_{\mathrm{H}}}{U})^2 + 2(\frac{3t}{U})^2}{\{1 + 3(\frac{J_{\mathrm{H}}}{U})^2 + 12(\frac{t}{U})^2\}^{\frac{3}{2}}}. \tag{C.6}$$

The latter three eigenvalues follow from the submatrix in equation (12).

References

[1] Kanamori J 1963 *Rep. Prog. Phys.* **30** 257
[2] Hubbard J 1963 *Proc. R. Soc.* A **276** 238
[3] Gutzwiller M C 1963 *Phys. Rev.* **10** 159
[4] Nagaoka Y 1966 *Phys. Rev.* **147** 392
[5] von der Linden W and Edwards D M 1991 *J. Phys.: Condens. Matter* **3** 4917
Becca F and Sorella S 2001 *Phys. Rev. Lett.* **86** 3396
[6] Hanisch T, Uhrig G and Müller-Hartmann E 1997 *Phys. Rev.* B **56** 13960
[7] Möller B, Doll K and Frésard R 1993 *J. Phys.: Condens. Matter* **5** 4847
[8] Byczuk K, Ulmke M and Vollhardt D 2003 *Phys. Rev. Lett.* **90** 196403
[9] Lieb E H 1989 *Phys. Rev. Lett.* **62** 1201
[10] Hirsch J E 1989 *Phys. Rev.* B **40** 2354
Hirsch J E 1991 *Phys. Rev.* B **43** 705
Kollar M, Strack R and Vollhardt D 1996 *Phys. Rev.* B **53** 9225
[11] Slater J C, Statz H and Koster G F 1953 *Phys. Rev.* **91** 1323
[12] Van Vleck J H 1953 *Rev. Mod. Phys.* **25** 220
[13] Oleś A M and Stollhoff G 1984 *Phys. Rev.* B **29** 314
Stollhoff G, Oleś A M and Heine V 1990 *Phys. Rev.* B **41** 7028
Held K and Vollhardt D 1998 *Eur. Phys. J.* B **5** 473
[14] Roth L M 1966 *Phys. Rev.* **149** 306
[15] Kugel K I and Khomskii D I 1973 *Sov. Phys.—JETP* **37** 725
[16] Cyrot M and Lyon-Caen C 1975 *J. Physique* **36** 253
[17] Inagaki S 1975 *J. Phys. Soc. Japan* **39** 596
[18] Maekawa S, Tohyama T, Barnes S E, Ishihara S, Koshibae W and Khaliullin G 2004 *Physics of Transition Metal Oxides* (Berlin: Springer)
[19] Oleś A M, Khaliullin G, Horsch P and Feiner L F 2005 *Phys. Rev.* B **72** 214431
[20] Feiner L F, Oleś A M and Zaanen J 1997 *Phys. Rev. Lett.* **78** 2799
Feiner L F and Oleś A M 1999 *Phys. Rev.* B **59** 3295
Di Matteo S, Jackeli G and Perkins N B 2003 *Phys. Rev.* B **67** 184427
Penc K, Mambrini M, Fazekas P and Mila F 2003 *Phys. Rev.* B **68** 012408
Mostovoy M V and Khomskii D I 2004 *Phys. Rev. Lett.* **92** 167201
Vernay F, Penc K, Fazekas P and Mila F 2004 *Phys. Rev.* B **70** 014428
Weisse A and Fehske H 2004 *New J. Phys.* **6** 158

Bala J and Horsch P 2005 *Phys. Rev.* B **72** 012404
[21] Khaliullin G and Maekawa S 2000 *Phys. Rev. Lett.* **85** 3950
Khaliullin G, Horsch P and Oleś A M 2001 *Phys. Rev. Lett.* **86** 3879
Di Matteo S, Perkins N B and Natoli C R 2002 *Phys. Rev.* B **65** 054413
Di Matteo S, Jackeli G, Lacroix C and Perkins N B 2004 *Phys. Rev. Lett.* **93** 077208
Khaliullin G, Horsch P and Oleś A M 2004 *Phys. Rev.* B **70** 195103
Di Matteo S, Jackeli G and Perkins N B 2005 *Phys. Rev.* B **72** 020408
[22] Frésard R and Kotliar G 1997 *Phys. Rev.* B **56** 12909
Bünemann J, Weber W and Gebhard F 1998 *Phys. Rev.* B **57** 6896
Klejnberg A and Spałek J 1998 *Phys. Rev.* B **57** 12041
Frésard R and Lamboley M 2002 *J. Low Temp. Phys.* **126** 1091
Koga A, Imai Y and Kawakami N 2002 *Phys. Rev.* B **66** 16
Florens S, Georges A, Kotliar G and Parcollet O 2002 *Phys. Rev.* B **66** 205102
Ōno Y, Potthoff M and Bulla R 2003 *Phys. Rev.* B **67** 035119
Pruschke T and Bulla R 2005 *Eur. Phys. J.* B **44** 217
Inaba K, Koga A, Suga A and Kawakami N 2005 *Phys. Rev.* B **72** 085112
[23] Liebsch A 2003 *Phys. Rev. Lett.* **91** 226401
Koga A, Kawakami N, Rice T M and Sigrist M 2004 *Phys. Rev. Lett.* **92** 216402
Liebsch A 2004 *Phys. Rev.* B **70** 165103
Ferrero M, Becca F, Fabrizio M and Capone M 2005 *Phys. Rev.* B **72** 205126
Knecht C, Blümer N and van Dongen P G J 2005 *Phys. Rev.* B **72** 081103(R)
Liebsch A 2005 *Phys. Rev. Lett.* **95** 116402
Inaba K, Koga A, Suga A and Kawakami N 2005 *J. Phys. Soc. Japan* **74** 2393
Rüegg A, Indergand M, Pilgram S and Sigrist M 2005 *Eur. Phys. J.* B **48** 55
Arita R and Held K 2005 *Phys. Rev.* B **72** 201102(R)
[24] Gill W and Scalapino D J 1987 *Phys. Rev.* B **35** 215
[25] Spałek J, Oleś A M and Chao K A 1979 *Physica* A **97** 552
[26] Kuei J and Scalettar R T 1997 *Phys. Rev.* B **55** 14968
[27] Hirsch J E 1997 *Phys. Rev.* B **56** 11022
[28] Daghofer M, Oleś A M and von der Linden M 2004 *Phys. Rev.* B **70** 184430
Daghofer M, Oleś A M and von der Linden M 2005 *Phys. Status Solidi* b **242** 311
[29] Sakamoto H, Momoi T and Kubo J 2002 *Phys. Rev.* B **65** 224403
[30] Xavier J C, Onishi H, Hotta T and Dagotto E 2006 *Phys. Rev.* B **73** 014405
[31] Koga A, Kawakami N, Rice T M and Sigrist M 2005 *Phys. Rev.* B **72** 045128
de' Medici L, Georges A and Biermann S 2005 *Phys. Rev.* B **72** 205124
Koga A, Inaba K and Kawakami N 2005 *Prog. Theor. Phys.* **160** 253
[32] Frésard R, Raczkowski M and Oleś A M 2005 *Phys. Status Solidi* b **242** 370
[33] Raczkowski M, Oleś A M and Frésard R 2005 *Physica* B **359** 672
[34] Goodenough J B 1963 *Magnetism and the Chemical Bond* (New York: Interscience)
Kanamori J 1959 *J. Phys. Chem. Solids* **10** 87
[35] Oleś A M, Horsch P, Feiner L F and Khaliullin G 2006 *Phys. Rev. Lett.* **96** 147205
[36] van der Brink J 2004 *New J. Phys.* **6** 201
Khaliullin G 2005 *Prog. Theor. Phys. Suppl.* **160** 155
[37] Sachan V, Buttrey D J, Tranquada J M, Lorenzo J E and Shirane G 1995 *Phys. Rev.* B **51** 12742
[38] Feiner L F and Oleś A M 2005 *Phys. Rev.* B **71** 144422
[39] Oleś A M 1983 *Phys. Rev.* B **28** 327
[40] Jorgensen J D, Dabrowski B, Pei S, Richards D R and Hinks D G 1989 *Phys. Rev.* B **40** 2187
[41] Radaelli P G, Hinks D G, Mitchell A W, Hunter B A, Wagner J L, Dabrowski B, Vandervoort K G, Viswanathan H K and Jorgensen J D 1994 *Phys. Rev.* B **49** 4163
[42] Sander K *et al* 1981 *Z. Anorg. Allg. Chem.* **480** 153
[43] Frischmuth B, Mila F and Troyer M 1999 *Phys. Rev. Lett.* **82** 835
van den Bossche M, Azaria P, Lecheminant P and Mila F 2001 *Phys. Rev. Lett.* **86** 4124
[44] Raczkowski M, Oleś A M and Frésard R 2006 unpublished
[45] Daré A-M, Hayn R and Richard J-L 2003 *Europhys. Lett.* **61** 803
[46] Raczkowski M, Frésard R and Oleś A M 2006 *Phys. Rev.* B **73** 094429